ARCHIVES OF ELECTRICAL ENGINEERING VOL. 64(3), pp. 427-439 (2015)

DOI 10.2478/aee-2015-0033

Flux-weakening control methods for hybrid excitation synchronous motor

HUANG MINGMING[1], GUO XINJUN[1], JIN PING[2], HUANG QUANZHEN[1], LIU YUPING[1], LI NA[1]

[1]*School of Electrical Information Engineering, Henan Institute of Engineering*
Zhengzhou, Henan 451191, China
e-mail: hngcxy_hmm@163.com

[2]*School of Energy and Electrical Engineering, Hohai University*
Nanjing 211100, China
e-mail: 15805158665@163.com

(Received: 27.10.2014, revised: 24.03.2015)

Abstract: The hybrid excitation synchronous motor (HESM), which aim at combining the advantages of permanent magnet motor and wound excitation motor, have the characteristics of low-speed high-torque hill climbing and wide speed range. Firstly, a new kind of HESM is presented in the paper, and its structure and mathematical model are illustrated. Then, based on a space voltage vector control, a novel flux-weakening method for speed adjustment in the high speed region is presented. The unique feature of the proposed control method is that the HESM driving system keeps the *q*-axis back-EMF components invariable during the flux-weakening operation process. Moreover, a copper loss minimization algorithm is adopted to reduce the copper loss of the HESM in the high speed region. Lastly, the proposed method is validated by the simulation and the experimental results.

Key words: hybrid excitation synchronous motor, wide speed range, vector control, flux-weakening control, current distributor

1. Introduction

The hybrid excitation synchronous motor (HESM) which is a wide speed-range machine derived from the permanent magnet synchronous motor (PMSM), contains two coexisting excitation sources: permanent magnet and excitation winding. The former generates the main air-gap magnetic flux and the latter produces the auxiliary one. Because of the excitation winding which can increase or reduce the flux of the air-gap magnetic field by changing the amplitude and direction of its current, the motor have the characteristics of low-speed high-torque and wide speed range. So, its applications are very extensive and valuable in the industry and agriculture, and particularly suitable for a certain kind of machines that requires a wide speed-range operational capabilities, such as electric vehicles, aerospace, computer numerical control (CNC) machine, and so on [1-5].

Due to the similarities of the structural and performance between the HESM and the PMSM, and also based on currently developed mature control technology and products of

PMSM, the basic principles and control methods of the PMSM can be fully absorbed for the HESM [6-9]. The HESM has an additional controllable excitation current which can be used for adjusting the air-gap magnetic field of the motor, so a reasonable allocation of the excitation current and the armature current must be integrally considered to achieve an optimal efficiency control and realize the excellent static and dynamic characteristics. The basic requirements of the control algorithm for the HESM are its operating performances of a larger starting torque and a low-speed high-torque when increasing air-gas magnetic field intensity (combination of the excitation current and the *d*-axis current for flux enhancement) under the rated speed, and the wide speed-range operation by reducing air-gas magnetic field intensity (combination of the excitation current and the *d*-axis current for flux-weakening) upon the rated speed. Currently, research papers about the HESM control system mainly include the followings: a fuzzy control scheme for a hybrid excitation brushless DC motor that is presented in [10], which regulates the *d*-axis current and the excitation current by a fuzzy controller; a dynamic vector control model based on a common coordinate system proposed by Shinji Shinnaka in [11] and a copper loss minimization vector control method based on $i_d = 0$ for a non-salient pole HESM in [12]; an excitation current self-optimization method based on the variable step-size search theory is proposed in [13] due to the nonlinear relationship between the field current and the electromagnetic torque; five different flux-weakening control strategies are analyzed and compared in [14] to obtain the optimal control method; a dynamic equivalent core losses resistance is applied to estimate the core loss in the *d*- and *q*-equivalent circuits in [15] to optimize the excitation current and the efficiency of HESM, considering the effect of the core loss .

Considering the aforementioned papers, in order to develop a HESM driving system with excellent performances, the key issue is to exploit a good flux-weakening control algorithm. As a result, according to the flux-weakening operating characteristics of the HESM in the high speed region, two control methods based on maintaining the back-EMF invariable are proposed. One is the copper loss minimization control method; the other is based on the use of the excitation current for flux-weakening control independently. By comparing the above two methods with the non-flux-weakening control method through simulations and experiments, it can be validated that the copper loss minimization control method have the widest speed range.

In Section 2, the framework and mathematical model of the HESM are presented. Next, two flux-weakening control algorithms for the HESM, especially the copper loss minimization control algorithm, are described in Section 3. The block diagram in Section 4 illustrates the motor control strategy and the simulation results are presented. The effectiveness of the proposed control method is validated by the experiment results show in Sections 5. Finally some conclusions are drawn in Section 6.

2. The structure and mathematical model of the HESM

The motor of the proposed HESM control system is a claw-pole asymmetric interlaced HESM, as shown in Figure 1, which is the dual stator structure and the outer stator is similar

to an ordinary PMSM's stator. Three-phase armature windings are installed inside; a chute structure is used to reduce cogging torque. The inner stator has a coil with an iron core, namely the excitation winding which fixed at the end cap of the HESM. The rotor appears in a claw-pole shape, the magnetically conductive irons (namely the iron-core pole) and the permanent magnets (namely the permanent magnet pole) on the adjacent claw-pole are placed in staggered arrangement. Inside of the HESM, the air-gas magnetic flux generated by the permanent magnet pole is almost unchanged during the running process. The air-gas magnetic flux generated by all currents components follows the direction of minor reluctance, in such a way that, their magnetic flux path is almost the same with the permanent magnet. The difference between the two magnetic sources is mainly based on the fact that the majority of the magnetic flux generated by the currents component is bypassed by the high magnetic conductivity material (iron core) which is paralleled with the permanent magnet, thus it won't pass through the permanent magnet and won't cause permanent damage to it. Based on the HESM topology, which has the iron-core poles, the excitation ability of the field winding is improved. Consequently, it can provide the high enhanced torque in the constant torque region and also widely extend speed range in flux-weakening operation.

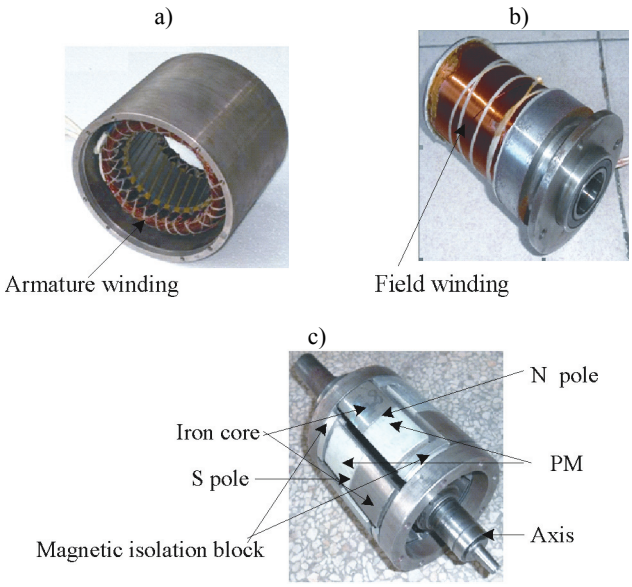

Fig. 1. The photo of HESM: a) the outer stator, b) the inner stator, c) the rotor

In summary, the paths of magnetic flux generated by the permanent magnets, the excitation current and the *d*-axis current are substantially identical. As a result, the air-gas magnetic flux produced by different magnetic sources can be almost linearly superimposed, and can also be effectively adjusted by changing the amplitude and direction of the excitation current and the *d*-axis current.

To simplify the analysis process, the effects of the harmonic components, temperature change, iron loss, stray loss, and magnetic saturation are ignored when the mathematical model and the driving system model are developed according to the aforementioned structure of the HESM. Several basic equations of the mathematical model of the HESM can be obtained as follows:

The circuit equation:

$$\begin{bmatrix} u_d \\ u_q \\ u_f \end{bmatrix} = \begin{bmatrix} R_s + sL_d & -\omega_e L_q & sM_{sf} \\ \omega_e L_d & R_s + sL_q & \omega_e M_{sf} \\ sM_{sf} & 0 & R_f + sL_f \end{bmatrix} \begin{bmatrix} i_d \\ i_q \\ i_f \end{bmatrix} + \begin{bmatrix} 0 \\ \omega_e \psi_{\text{pm}} \\ 0 \end{bmatrix}. \tag{1}$$

The flux linkage equation:

$$\begin{bmatrix} \psi_d \\ \psi_q \end{bmatrix} = \begin{bmatrix} L_d & 0 & M_{sf} \\ 0 & L_q & 0 \end{bmatrix} \begin{bmatrix} i_d \\ i_q \\ i_f \end{bmatrix} + \begin{bmatrix} \psi_{\text{pm}} \\ 0 \end{bmatrix}. \tag{2}$$

The torque equation:

$$\begin{aligned} T_e &= \frac{3}{2} p(i_q \psi_d - i_d \psi_q) \\ &= \frac{3}{2} p i_q [\psi_{\text{pm}} + i_d (L_d - L_q) + M_{sf} i_f]. \end{aligned} \tag{3}$$

In the formula (1)-(3), the symbol meanings are as the following: u_d – d-axis voltage component, u_q – q-axis voltage component, i_d – d-axis current component, i_q – q-axis current component, ψ_d – d-axis flux linkage, ψ_q – q-axis flux linkage, ψ_{pm} – the flux linkage generated by permanent magnet , u_f – excitation voltage, i_f – excitation current, R_s – armature resistance, R_f – excitation winding resistance, L_d – d-axis inductance, L_q – q-axis inductance, M_{sf} – mutual inductance between armature winding and excitation winding, ω_e – electrical angular velocity, p – number of pole pairs of the motor, T_e – electromagnetic torque.

3. Flux-weakening control algorithms for the HESM

The HESM enters into the high-speed operation mode when its speed n_r exceeds the flux-weakening base speed n_{Bdec}, while the back-EMF is approaching to the voltage of power supply. If further to elevate the speed, a certain flux-weakening control method must be used. The amplitude regulation of the armature current and excitation current is restricted to the voltage limit ring, which is similar to the PMSM flux-weakening control method in the constant power region. When the HESM operates in steady-state, the magnitude of voltage vector has to meet the following as

$$u_s^2 = u_d^2 + u_q^2 \le U_{\text{lim}}^2 . \tag{4}$$

where, U_{lim} is the maximum value of the voltage vector, its value depends on the bus voltage of the drive circuit U_{dc}. Generally, the value of u_q is approaching to u_s when the motor operates in steady-state in the high-speed region, and simultaneously it is determined by the q-axis component of the back EMF (E_q). According to the above analysis, a flux weakening control method based on keeping the back EMF invariable is obtained

$$E_q = E_{\text{base}} , \tag{5}$$

where, E_{base} is the value of the back-EMF in the no-load condition when n_r reaches n_{Bdec}, it can be obtained by

$$E_{\text{base}} = pn_{\text{Bdec}}\psi_{\text{pm}}\pi / 30 \tag{6}$$

E_q can be expressed as

$$E_q = \frac{p\pi n_r}{30}(\psi_{\text{pm}} + i_d L_d + i_f M_{sf}) . \tag{7}$$

Obviously, there is a linear relationship between E_q and n_r if let $i_d = i_f = 0$. Therefore, when adopting the conventional vector control, the maximum speed n_{max}, which is obtained in no-load and no field current condition, is also linear with U_{dc}. Furthermore, n_{Bdec} is limited by n_{max} which is obtained by experiments based on using the vector control with $i_d = i_f = 0$ and in the no-load condition. Then, the relationships between n_{Bdec}, n_{max} and U_{dc} can be derived by

$$\begin{cases} n_{\text{max}} = k_v U_{\text{dc}} + N_0 \\ n_{\text{Bdec}} = k_{\text{b}} n_{\text{max}} \end{cases} , \tag{8}$$

where, according to the experimental prototype, the coefficient $k_v = 5.69$, the offset value $N_0 = -13$. To ensure the utilization rate of the DC bus voltage and the HESM's efficiency in the flux-weakening operation state, the coefficient k_{b} is set at a range between 0.7 and 0.9 (in this paper, $k_b = 0.75$). Such, when we let $U_{\text{dc}} = 300$ V, the value of n_{Bdec} can be obtained, namely $n_{\text{Bdec}} = 1270$ rpm.

Therefore, in order to maintain the back EMF in a higher value and unchanged in the flux-weakening operation state, by combining the Equations (5-7), the following equation can be derived

$$(L_d i_d + M_{sf} i_f) = \frac{\psi_{\text{pm}}(n_{\text{Bdec}} - n_r)}{n_r} . \tag{9}$$

There are two variables in (9), in order to get the unique solutions of i_d and i_f, we have to build another equation. Considering optimizing the efficiency of the HESM, a copper loss minimization control algorithm is adopted. To simplify the computation, the q-axis current is

directly determined by the speed controller. Such, the simplified copper loss equation without considering the *q*-axis current as follows

$$P_{\mathrm{cu}} = \frac{3}{2} i_d^2 R_s + i_f^2 R_f \,. \tag{10}$$

To get the reference currents, based on the copper loss minimization algorithm, let $i_d = i_{dref}$ and $i_f = i_{fref}$ and combining (9-10), the Lagrange multiplier method is adopted

$$L(i_{\mathrm{dref}}, i_{\mathrm{fref}}, \lambda) = P_{\mathrm{cu\_ref}} + \lambda[(L_d i_{\mathrm{dref}} + M_{sf} i_{\mathrm{fref}}) - \frac{\psi_{\mathrm{pm}}(n_{\mathrm{Bdec}} - n_r)}{n_r}] \,. \tag{11}$$

To solve partial derivative of i_{dref}, i_{fref} and λ for Equation (11), respectively

$$\begin{cases} \dfrac{\partial L}{\partial i_{\mathrm{dref}}} = 3 i_{\mathrm{dref}} R_s + \lambda L_d \\ \dfrac{\partial L}{\partial i_{\mathrm{fref}}} = 2 i_{\mathrm{fref}} R_f + \lambda M_{sf} \\ \dfrac{\partial L}{\partial \lambda} = (L_d i_{\mathrm{dref}} + M_{sf} i_{\mathrm{fref}}) - \dfrac{\psi_{\mathrm{pm}}(n_{\mathrm{Bdec}} - n_r)}{n_r} \end{cases}, \tag{12}$$

where, assuming

$$\frac{\partial L}{\partial i_{\mathrm{dref}}} = 0 \,, \quad \frac{\partial L}{\partial i_{\mathrm{fref}}} = 0 \,, \quad \frac{\partial L}{\partial \lambda} = 0 \,,$$

the reference currents are obtained as the following

$$\begin{cases} i_{\mathrm{dref}} = -\dfrac{L_d}{3R_s} \lambda \\ i_{\mathrm{fref}} = -\dfrac{M_{\mathrm{sf}}}{2R_f} \lambda \end{cases}, \tag{13}$$

where

$$\lambda = \frac{6 R_s R_f \psi_{\mathrm{pm}} (n_r - n_{\mathrm{Bdec}})}{n_r (2 R_f L_d^2 + 3 R_s M_{sf}^2)} \,. \tag{14}$$

In summary, two current allocation algorithms can be used in the flux-weakening control for the HESM.

Algorithm 1, adopting the flux-weakening control based on the copper loss minimization algorithm, the reference values for each current component are the following as

$$\begin{cases} i_{\text{qref}} = k_i T_{\text{eref}} \\ i_{\text{dref}} = -\dfrac{L_d}{3R_s}\lambda \\ i_{\text{fref}} = -\dfrac{M_{\text{sf}}}{2R_f}\lambda \end{cases}, \tag{15}$$

where, T_{eref} is obtained directly by the speed controller as shown in Figure 2.

Algorithm 2, using only the excitation current for the flux-weakening control, namely based on the vector control with $i_{\text{dref}} = 0$ to adjust speed, from the Equation (9), the reference values of current component can be obtained by

$$\begin{cases} i_{\text{qref}} = kT_{\text{eref}} \\ i_{\text{dref}} = 0 \\ i_{\text{fref}} = \dfrac{\psi_{pm}}{M_{sf}}\left(\dfrac{n_{Bdec}}{n_r} - 1\right) \end{cases}. \tag{16}$$

4. Modeling and simulation

In order to verify the effectiveness of the flux-weakening control method, the driving system model of HESM is developed by using MATLAB/SIMULINK, shown in Figure 2.

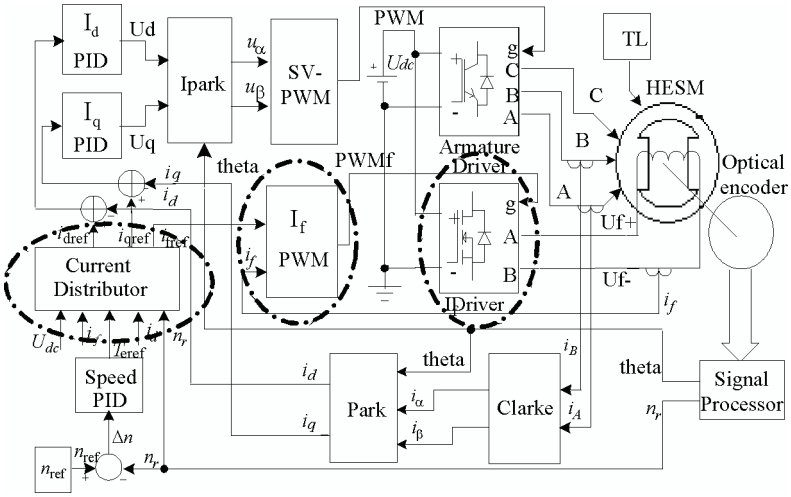

Fig. 2. HESM control system model

The main function modules include a HESM sub-module, a Clarke sub-module, a Park sub-module, an Ipark sub-module, a Speed PID sub-module, a Current Distributor sub-module, an

I_d PID sub-module, an I_q PID sub-module, a SVPWM sub-module, an I_f PWM sub-module, an Armature Driver sub-module and an I_f Driver sub-module. Comparing with the traditional PMSM vector control system, the HESM control system adds 3 functional sub-modules, which are the I_f PWM sub-module, the I_f Driver sub-module and the Current Distributor sub-module, respectively. The I_f PWM sub-module outputs control signals to control the I_f Driver, and its control principle is shown in Figure 3. The I_f Driver sub-module is a single-phase bridge inverter circuit which is applied for producing the excitation current. The Current Distributor sub-module is used for current regulating, and it divides the whole speed-operation range into two regions, which are the low speed region and the high speed region, respectively, as shown in Figure 4.

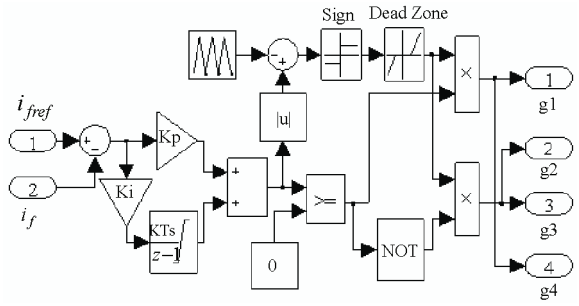

Fig. 3. Control signal generating module for I_f PWM

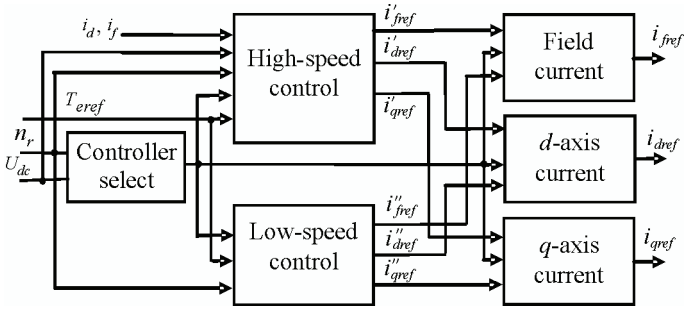

Fig. 4. Current allocation module

Table 1. Characteristic parameters of the prototype

Parameters	Value	Parameters	Value	Parameters	Value
P_N (W)	700	U_{dc} (V)	300	Ψ_{pm} (Wb)	0.243
n_N (rpm)	500	R_s (Ω)	2.7	p	4
T_N (Nm)	13	R_s (Ω)	33.0	M_{sf} (mH)	76
I_N (A)	5	L_q(mH)	27	L_d (mH)	38
I_{fN} (A)	1.0	L_f (H)	0.57		

Notes: P_N , n_N, T_N, I_N, I_{fN} are rated output power, rated speed, rated torque, rated armature current, rated excitation current respectively.

According to the control system model shown in Figure 2, the following simulation analysis is carried out in detail. The simulation results of three different control methods are compared, which include the non-flux-weakening control method, with only the excitation current for the flux-weakening control method and the copper loss minimization control method which utilizes the *d*-axis current and the excitation current together for flux weakening. The simulation parameters of the HESM are set up according to the actual parameters of the prototype, as shown in Table 1.

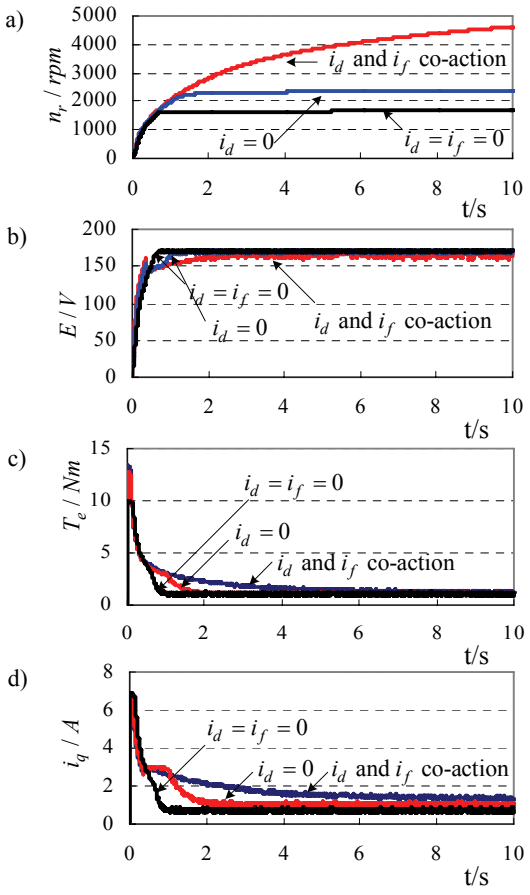

Fig. 5. Simulation curves for HESM

Figure 5 shows the comparison results of simulation curves of the three different kinds of control strategies, which adopt the vector control with $i_{dref} = i_{fref} = 0$, $i_{dref} = 0$, and the copper loss minimization (i_f and i_d co-action), respectively. The load is set to 1Nm and the reference speed is set to 6000 rpm. Figure 5 a) is the speed curves produced by the three different

control methods. Adopting the non-flux-weakening control algorithm, the maximum speed is 1650 rpm; adopting with only i_f for the flux-weakening control algorithm, the maximum speed is 2350 rpm; adopting the copper loss minimization control algorithm for the flux-weakening control, the maximum speed is more than 4600 rpm. Figure 5 b) is the back-EMF curves of the three different control methods. It is obviously that the back-EMF curve produced by the non-flux-weakening control method increased to the peak fastest, and the back EMF curve produced by the copper loss minimization control method increased slowest. Finally, all of them rose to 160 V~170 V as the HESM entered into the steady-state. Figure 5 c) is the electromagnetic torque T_e curves produced by the three different control methods. Figure 5 d) is the i_q curves produced by the three different control methods.

5. Experimental results

According to the proposed HESM control methods and the simulation results, a HESM controller based on TMS320F2812 + AT89C55WD architecture is set up, and the driving experiments are carried out correspondingly.

Figure 6 shows the experimental photo of the HESM driving system. The rated DC bus voltage for the experimental prototype is 300 V. The motor torque characteristics testing adopt a TS-7700 Torque Station Pro with MT-6425 torque detectors. This set of equipment can be used to measure the motor speed, torque, input and output power and efficiency. The prototype of the HESM is an asymmetric staggered construct and has an incremental optical encoder disk, TAMAGAWA OIH48-2500, which is built in the motor. The controller includes four circuit boards: the first is a dashboard; the second is the control circuit board which is based on TMS320F2812 + AT89C55WD; the third and fourth are two driving boards which are used for producing the armature current and the excitation current, respectively.

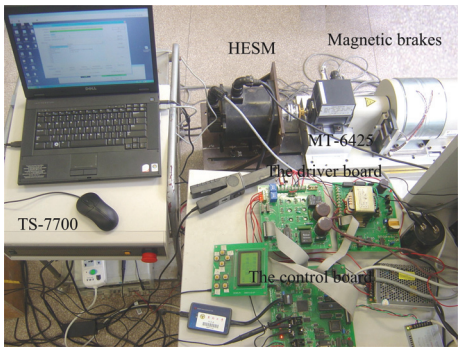

Fig. 6. The HESM experiment setup

Figure 7 shows the current waveforms of the HESM during starting process. The load is 1 Nm; the given speed is 2800 rpm which is greater than the flux-weakening base speed (1270 rpm) of the HESM. In order to improve the starting torque of the motor, considering the

excitation winding's inductance is larger, a rated positive excitation current is applied to the excitation winding before 0.5 s to switch on the armature current. As the motor speed increasing, the excitation current decreases gradually. When speed reaches n_{Bdec}, the stage of the flux-weakening control for the speed adjusting begins, and i_f and i_d continually decrease as the speed rise.

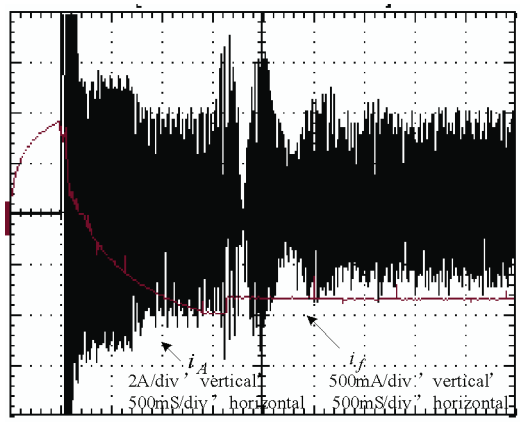

Fig. 7. Current waveforms in the starting process

Figure 8 shows steady current waveforms of the HESM in the flux-weakening operation with the copper loss minimization method. The given speed is 2800 rpm, the load torque is 1 Nm, and the excitation current i_f is −0.8 A, which remains basically a constant. The amplitude of the sine-wave phase current which is smooth, low harmonics is 4 A.

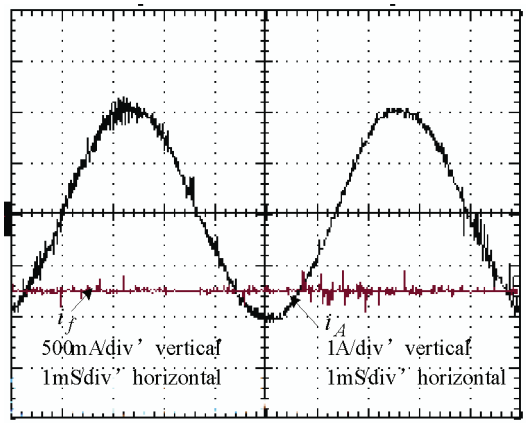

Fig. 8. Steady-state current waveforms in flux-weakening operation

Figure 9 shows the curves of the maximum output power vs. speed by the three different control methods. Adopting the non-flux-weakening ($i_d = i_f = 0$) control method, the constant power speed range is approximately from 700 rpm to 1300 rpm. Adopting the method that

applies only the excitation current i_f ($i_d = 0$) for the speed adjustment, it generates a constant power speed range between 450 rpm and 1600 rpm. When adopting the copper loss minimization algorithm for the flux-weakening control method, the constant power speed range extends from 450 rpm to 2000 rpm; when the speed exceeds 2000 rpm, although the output power cannot be constant, it decreases slowly and the output power drops to about 200 W as the speed rises to 4000 rpm. The experimental results show that applying the copper loss minimization algorithm for the flux-weakening control can extend the speed range of HESM effectively.

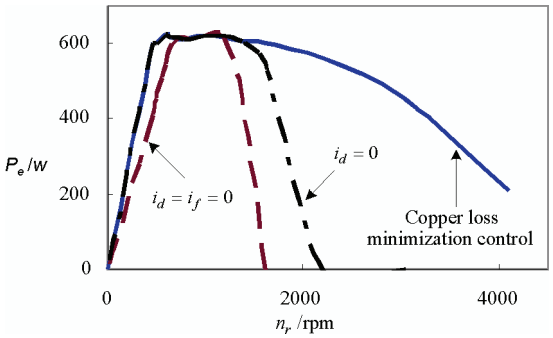

Fig. 9. The maximum output power at different speeds

6. Summary

In this paper, the structure and mathematical model of a novel HESM is presented. With the additional field winding, the HESM has excellent air-gas magnetic field adjustment capability. Based on the vector control technique and the copper loss minimization algorithm, a new flux-weakening control method is proposed. The proposed method adopts the way of regulating the armature and the excitation current in the high speed region by keeping the q-axis back EMF invariable. To validate the proposed control method, simulations and experiments were carried out, and three different control methods, including the non-flux-weakening control, with just i_f for the flux-weakening control, and the copper loss minimization control have been compared. The results show that adopting the copper loss minimization algorithm for the flux-weakening control has the widest speed-range operation.

Acknowledgment

This work was supported by Scientific and technological project of Henan Science and Technology Agency(142102210403). Project Supported by the National Natural Science Foundation of China (61403123), Project Supported by the Doctoral Fund of Henan Institute of Engineering(D2014012).

References

[1] May H., Palka R., Paplicki P. et al., *Modified concept of permanent magnet excited synchronous machines with improved high-speed features*. Archives of Electrical Engineering 60(4): 531-540 (2011).

[2] Di B.P., Mognaschi M.E., Palka R. et al., *Design optimization of a permanent-magnet excited synchronous machine for electrical automobiles.* International Journal of Applied Electromagnetics and Mechanics 39(1): 889-895 (2012).
[3] Yang C.F., Lin H.Y., Guo J., Zhu Z.Q., *Design and analysis of a novel hybrid excitation synchronous machine with asymmetrically stagger permanent magnet.* IEEE Transactions on Magnetics 44(11): 4353-4356 (2008).
[4] Chan C.C., Chau K.T., Jiang J.Z. et al., *Novel permanent magnet motor drives for electric vehicles*. IEEE Transactions on Industrial Electronics 43(2): 331-339 (1996).
[5] Liu X.P., Chen D., Yi L. Zhang C., Wang M., *Comparison and analysis of magnetic-geared permanent magnet electrical machine at no-load*. Archives of Electrical Engineering 63(4): 683-692 (2014).
[6] Chen J.J., Chin K.P., *Minimum copper loss flux weakening control of surface mounted permanent magnet synchronous motors*. IEEE Transactions on Power Electronics 18(4): 929-936 (2003).
[7] Lawler J.S., Bailey J., McKeever J., *Minimum current magnitude control of surface PM synchronous machines during constant power operation*. IEEE Power Electronics Letters 3(2): 53-56 (2005).
[8] Fuchs E.F., Myat M.H., *Speed and torque range increases of electric drives through compensation of flux weakening*. International Symposium on Power Electronics, Electrical Drives, Automation and Motion, Pisa, Italy, SPEEDAM: 1569-1574 (2010).
[9] Chen J.J., Chin K.P., *Automatic flux-weakening control of permanent magnet synchronous motors using a reduced-order controller*. IEEE Transactions on Power Electronics 15(5): 881-890 (2000).
[10] Chan C.C., Zhang R., Chau K.T., *Optimal efficiency control of PM hybrid motor drives for electrical vehicles*. Power Electronics Specialists Conference, St. Louis, USA, pp. 363-368 (1997).
[11] Shinnaka S., *New dynamic mathematical model and new dynamic vector simulators of hybrid-field synchronous motors*. IEEE International Conference on Electric Machines and Drives, San Antonio, TX, USA, pp. 882-889 (2005).
[12] Shinnaka S., *New optimal current control methods for energy-efficient and wide speed-range operation of hybrid-field synchronous motor*. IEEE transactions on industrial electronics 54(5): 2443-2450 (2007).
[13] Wang W.J., Zhang Z.R., *Maximum torque control of hybrid excitation synchronous machine drives based on field current self-optimizing method.* IECON Proceedings: 2977-2982 (2013).
[14] Capponi, F.G., Borocci G., Donato D., Caricchi, F. *Flux Regulation Strategies for Hybrid Excitation Synchronous Machines.* Energy Conversion Congress and Exposition (ECCE), 2014 IEEE: 4858-4865 (2014).
[15] Kong L., Wen X.H., Fan T., *A New Method to Plan the Optimal Field Excitation Current Trajectory in a Hybrid Excitation Machine.* 2011 International Conference on Electrical Machines and Systems: 1-4 (2011).